

Review

# Recent Progress in Green Conversion of Biomass Alcohol to Chemicals via Aerobic Oxidation

Yifei Zhang <sup>1,2</sup>, Changhai Cao <sup>3,\*</sup> and Gao Li <sup>2,\*</sup> 

<sup>1</sup> Institute of Catalysis for Energy and Environment, College of Chemistry and Chemical Engineering, Shenyang Normal University, Shenyang 110034, China; sszyf2017@126.com

<sup>2</sup> State Key Laboratory of Catalysis, Dalian Institute of Chemical Physics, Chinese Academy of Sciences, Dalian 116023, China

<sup>3</sup> Key Laboratory of Biofuels and Biochemical Engineering, SINOPEC Dalian Research Institute of Petroleum and Petro-Chemicals, Dalian 116045, China

\* Correspondence: caochanghai.fshy@sinopec.com (C.C.); gaoli@dicp.ac.cn (G.L.)

**Abstract:** The aerobic oxidation of biomass transformations into valuable chemical products via a green catalytic process is one of the most important protocols because of its low reaction temperature and high productivity rate. Recently, the introduction of small-sized Cu and Au nanoparticles (e.g., 1–3 nm) upon the surface of oxides can provide more catalytic active sites and then enhance the catalytic activity of aerobic oxidations significantly. The introduction of these metal nanoparticles is a kind of perfect catalyst for enhancing the efficiency of the activation of oxygen molecules and the separation of photo-generated holes and electrons during the photo-oxidation reactions. In this account, we summarize recent progress of the aerobic oxidation of biomass alcohol toward the production of highly valuable chemicals over supported catalysts of metal nanoparticles (NPs), including methanol conversion into methyl formate via photo-oxidation over CuO<sub>x</sub>/TiO<sub>2</sub> nanocomposites, biomass ethanol transformation with biomass furfural to produce hydrocarbons biofuels over Au/NiO catalysts, and glucose oxidation to gluconic acid using Au/activated carbon (Au/AC) as catalysts. Furthermore, at the atomic level, to understand the structure-property correlations, insights into molecular activations of oxygen and biomass, and the investigation of active catalytic sites on photo/catalysts will be detailed and discussed. Finally, future studies are needed to achieve more exciting progress in the fundamental revealing of the catalytic reaction mechanisms and conversion pathway and the future perspective in industrial applications.

**Keywords:** biomass; Au; Cu; methanol; ethanol; D-glucose; valuable chemicals; aerobic oxidation



**Citation:** Zhang, Y.; Cao, C.; Li, G. Recent Progress in Green Conversion of Biomass Alcohol to Chemicals via Aerobic Oxidation. *Biomass* **2022**, *2*, 103–115. <https://doi.org/10.3390/biomass2020007>

Academic Editor: S David Jackson

Received: 15 April 2022

Accepted: 13 May 2022

Published: 16 May 2022

**Publisher's Note:** MDPI stays neutral with regard to jurisdictional claims in published maps and institutional affiliations.



**Copyright:** © 2022 by the authors. Licensee MDPI, Basel, Switzerland. This article is an open access article distributed under the terms and conditions of the Creative Commons Attribution (CC BY) license (<https://creativecommons.org/licenses/by/4.0/>).

## 1. Introduction

With the increase in the energy demands for future societies, biomass methanol and ethanol as sustainable energy attract enormous attention as a secure method for solving energy demands [1,2]. Methyl formate (HCOOCH<sub>3</sub>) produced from methanol and hydrocarbons from biomass ethanol with biomass furfural has been considered an environmentally benign valuable chemical product with the novel area called “green chemistry”, which has been used as an important precursor to produce pharmaceuticals and pesticides and as an additive to petroleum in the chemical industry [3–5].

Traditionally, methyl formate was industrially produced via carbonylation and dehydrogenation processes with methanol as raw material at high elevated temperatures (>100 °C), which is usually with low selectivity as the generation of many different by-products, e.g., formaldehyde (HCHO), dimethoxymethane, dimethyl ether (DME), carbon oxides (CO and CO<sub>2</sub>), etc., thereby posing a major issue for further separation and extra expenses [6–8]. Thus, the green photo-oxidation of methanol at ambient temperature showed great advantages and considerable prospects for the large-scale synthesis of methyl

formate due to the green and energy saving nature of the pathway with a few CO<sub>2</sub> formations (e.g., <5%) [9]. Of note, the CO<sub>2</sub> formation is more than 10% at a higher reaction temperature in the thermal conversions of methanol.

As a kind of liquid fuel, hydrocarbons are the outmost important source of motive power energy in the field of the transportation sector, being produced on an industrial scale from nonrenewable fossil-based resources now. With the depletion of oil, the manufacture of sustainable biofuels from biomass has attracted particular interest. Bioethanol is a kind of important biomass that is renewable and a green chemical and commonly known as “cellulosic ethanol”, which can be produced from various plant materials [10] and react with an aldehyde via aldol condensation that is an effective protocol for C–C bond formation to produce biofuels [11–14]. Therefore, these conversion pathways by the ethanol oxidation condensation may provide an important breakthrough for diversification and sustainable development of hydrocarbon biofuels production [15–17].

With the aim of minimizing the consumption of fossil fuels and reducing CO<sub>2</sub> emission, the transformation of renewable biomass-derived natural resources into corresponding high valuable biofuels and bio-chemicals is also another appealing and sustainable protocol [18–22]. For instance, the catalytic selective aerobic oxidation of glucose into gluconic acid or salts is one of the most important green chemical reactions [23]; it is an important commercial chemical that could be widely applied in many fields, such as food additives, raw material for the medicine, polymer manufacture, a few to name. At present, the industrial production of gluconic acid and its salts depends on microbial production or the aerobic oxidation process of glucose catalyzed by the Pd-based catalysts with loading Bi or Pb [24,25]. The Bi and Pb additives would contaminate the gluconic acid products (e.g., the residual Bi and Pb cations from the catalysts) [25], and it results in further purifications and the generation of waste.

Herein, we introduce recent progress in the green transformations of biomass to valuable chemicals, including the photo-oxidation of methanol toward the production of methyl formate over CuO<sub>x</sub>/TiO<sub>2</sub> catalysts in the gas phase and the production of glucuronic acid from glucose via aerobic oxidation over Au/AC (AC: activated carbon) in a liquid phase and the hydrocarbon production from ethanol with furfural via a one-pot cascade reaction catalyzed by Au/NiO, *viz.*, cross aldol condensations and then hydrogenolysis process. Moreover, the extrapolate catalytic mechanisms, and reaction pathways are thoroughly discussed based on systems developed mainly in our lab till April 2022.

## 2. Methanol Conversion to Methyl Formate

Methyl formate is one of the most important chemicals, which is widely used as synthesis intermediates, solvent for cellulose, and fumigants and fungicides in industrial productions [26,27]. Global consumption has largely increased by an average of ~9%/year from ~6.2 million tons in 2015 to 8.4 million tons in 2019, Figure 1.



As can be seen from Equation (1), the value of  $\Delta H$  for methanol oxidation into methyl formate product is  $-102.5 \text{ kcal mol}^{-1}$ , so it is a strongly exothermic reaction, indicating that the photocatalytic methanol oxidation is feasible [28]. The gas phase photocatalytic methanol oxidation process was schematically illustrated in Figure 2 [29]. The bare anatase-TiO<sub>2</sub> showed inferior photoactivity [30,31], although the apparent energy of activation is some low ( $\sim 6.1 \text{ kJ mol}^{-1}$ ), which is much lower than these over the transition metal oxides in the thermal oxidation ( $39\text{--}126 \text{ kJ mol}^{-1}$ ). Thus, the extent of photocatalysis to the Cu/TiO<sub>2</sub> system was developed [32]. As the work function of Cu ( $\varphi_{\text{Cu}} = 4.60 \text{ eV}$  [33]) is very close to that of TiO<sub>2</sub> ( $\varphi_{\text{TiO}_2} = 4.70 \text{ eV}$ ), an Ohmic contact can be formed on the surface of TiO<sub>2</sub> and Cu in the Cu/TiO<sub>2</sub> complex nanomaterial.

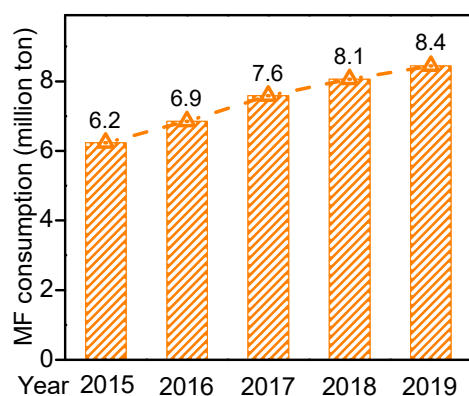


Figure 1. The global consumption of methyl formate update to 2019.

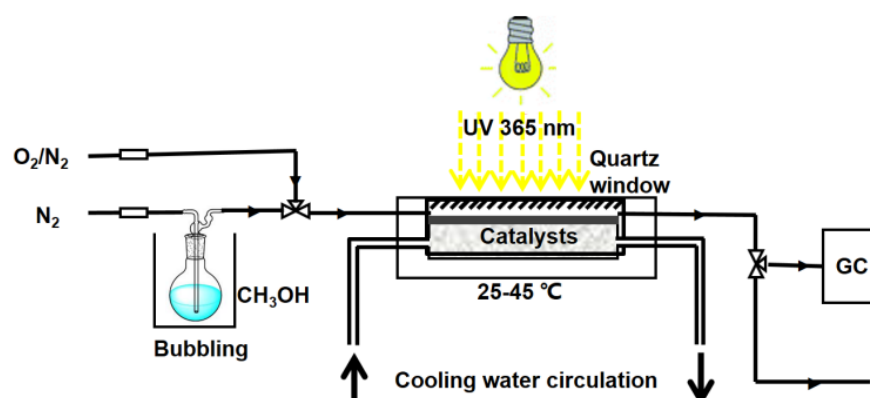
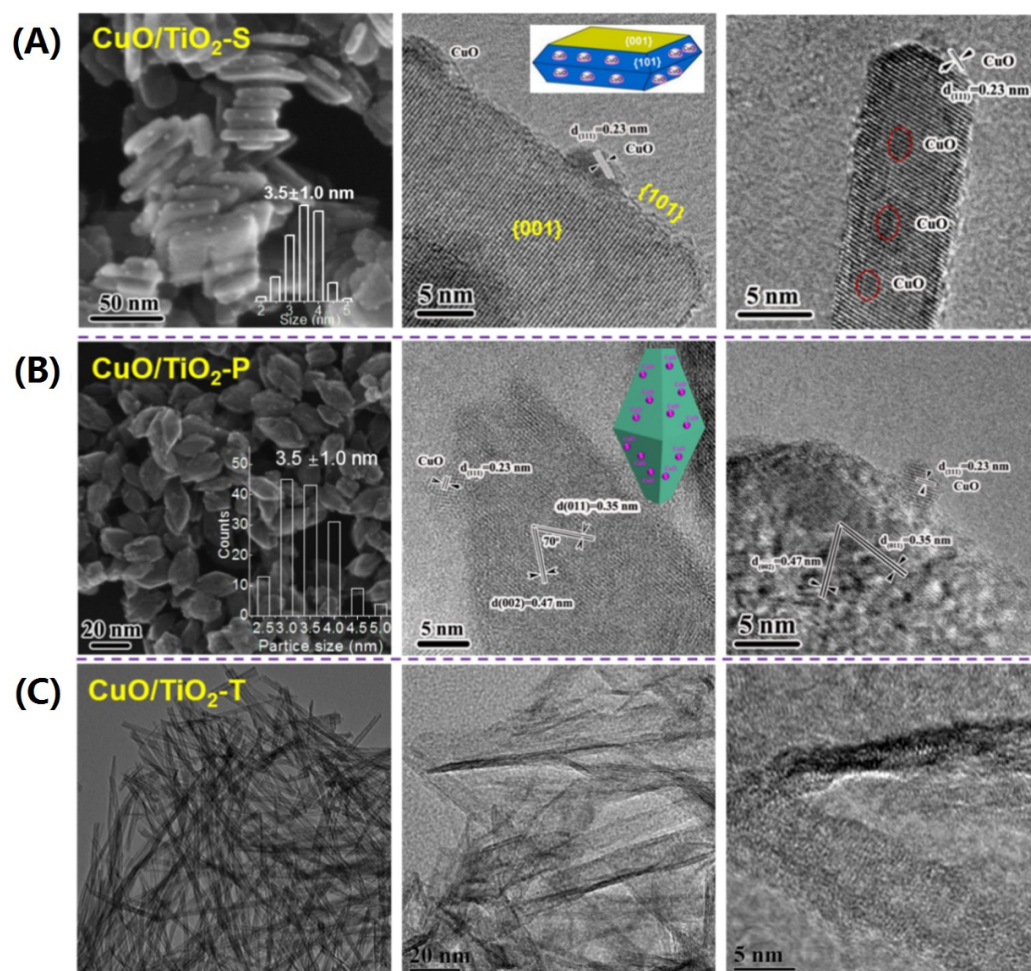


Figure 2. Schematic system of photo-oxidation. Reproduced with permission from Ref. [29]. Royal Society of Chemistry, 2019.

The previous studies only focused on anatase-TiO<sub>2</sub> or P25 (a mixture of anatase phase and rutile phase of TiO<sub>2</sub>) as support for metal nanoparticles (NPs), which cannot be used to go insight the interfacial perimeter of the oxide supports and metal NPs. Note that the interfacial perimeter of the oxide supports and metal NPs is often deemed as the catalytically active sites during the metal NPs-catalyzed reactions. In the past decades, the TiO<sub>2</sub> with various shapes (such as nanorods (R), nanosheets (S), nanospindles (P), nanotube (T), etc.) has been successfully synthesized [34,35]. These well-defined TiO<sub>2</sub>s have specific exposing facets. For example, TiO<sub>2</sub>{001} and TiO<sub>2</sub>{101} surfaces are observed in the TiO<sub>2</sub>-S sample (Figure 3A), which has been widely used as photocatalysts [36,37], and very recently, CuO<sub>x</sub>/TiO<sub>2</sub>-S heterojunction was prepared via a reduction-deposition method as a well-defined and efficient photocatalyst and used for the photo-oxidation of methanol to methyl formate with oxygen (O<sub>2</sub>) gas as the oxidant [29]. The CuO<sub>x</sub> particles with small-sized (~3.5 nm, Figure 3A) were selectively supported on the TiO<sub>2</sub>{101} interface of anatase-TiO<sub>2</sub>-S, which can reduce the recombination of photo-generated electrons/holes dramatically under the situation of light irradiation. The CuO/TiO<sub>2</sub>-S heterojunction catalysts exhibited an excellent catalytic behavior under mild conditions for the catalytic photo-oxidation of methanol. The conversion is promoted by increasing reaction temperatures, and simultaneously the selectivity for methyl formate decreases.

Then, the concentration of the CuO<sub>x</sub> loading was further investigated. It could be found that CuO<sub>x</sub>/TiO<sub>2</sub> photocatalyst with 5 wt% showed the best catalytic performance (~95% conversion and >85% selectivity for methyl formate), as shown in Figure 4. Interestingly, CO<sub>2</sub> and formaldehyde by-products were observed in the reactions in the presence of 0.3% O<sub>2</sub>, and more CO<sub>2</sub> was found when the O<sub>2</sub> concentration improved to 0.75% and 1.0%, based on the conversion and selectivity in this photocatalytic reaction system, 0.5% O<sub>2</sub> is the most suitable concentration. The reaction rate for methyl formate production at the optimal conditions can reach up to be 10.8 mmol·g<sup>-1</sup>·h<sup>-1</sup> at ambient temperature, which

is remarkably higher than only used bare  $\text{CuO}_x$  oxides or  $\text{TiO}_2\text{-S}$ . The robust  $\text{CuO}_x/\text{TiO}_2\text{-S}$  nanocomposites showed excellent durability for over 20 h. The unique electronic structure of oxide catalysts led to superior activity, and the synergistic effects of  $\text{CuO}_x/\text{TiO}_2$  also improved the activity effectively.



**Figure 3.** TEM images of the  $\text{CuO}/\text{TiO}_2$  with different morphologies: (A)  $\text{CuO}/\text{TiO}_2\text{-S}$ , (B)  $\text{CuO}/\text{TiO}_2\text{-P}$ , and (C)  $\text{CuO}/\text{TiO}_2\text{-T}$ . Reproduced with permission from Refs. [29,38,39]. Royal Society of Chemistry, 2019. Springer, 2020, and American Society of Chemistry, 2020.

Next, Shi et al. further deposited the  $\text{CuO}_x$  nanoclusters onto the side  $\text{TiO}_2\{101\}$  plane of the  $\text{TiO}_2\text{-P}$  (Figure 3B) [38]. Note that there was not enough space on the top of  $\text{TiO}_2\text{-P}$  to anchor the  $\text{CuO}_x$  nanoclusters. Methanol-TPD experiments showed methanol could be chemisorbed on the surface of the  $\text{CuO}/\text{TiO}_2$  catalyst. It means the  $\text{CuO}/\text{TiO}_2$  should be an excellent candidate for the methanol oxidation reactions. An > 97% conversion and 83% selectivity were obtained over the  $\text{CuO}/\text{TiO}_2\text{-P}$  under mild conditions. Interestingly, the surface oxygen vacancy ( $\text{O}_V$ ) species have a big influence on catalytic activity during the  $\text{CuO}/\text{TiO}_2\text{-P}$  catalyzed reactions [39,40], Figure 4E. Thus, the small-sized  $\text{CuO}$  particles can optimally tune excitons recombination by  $\text{O}_V$  generation and then promote its catalytic activity. Further, for the first time, in situ attenuated total reflection infrared (ATR-IR) spectroscopic analysis reveals the adsorbed methoxy ( $\text{CH}_3\text{O}^*$ ) was converted to adsorbed formaldehyde ( $\text{CHO}^*$ ) species in the presence of oxygen (Scheme 1, (3)) in the methanol conversion, Figure 5A,B. Then formed  $\text{CHO}^*$  species further reacted with a neighboring  $\text{CH}_3\text{O}^*$  to provide methyl formate [38].

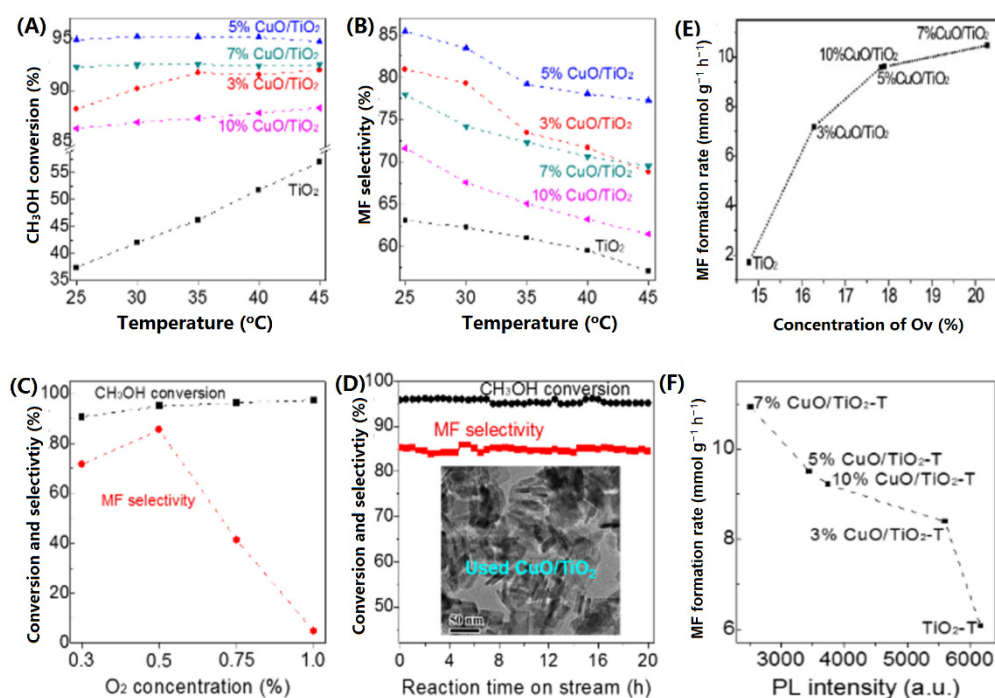


**Figure 4.** (A)  $\text{CH}_3\text{OH}$  conversion and (B) selectivity toward methyl formate over  $\text{CuO}/\text{TiO}_2\text{-S}$ . (C) The catalytic performances at different  $\text{O}_2$  concentrations. (D) Durability test. Relationship of formation rate of methyl formate (MF) with (E) the concentration of  $\text{O}_\text{V}$  and (F) PL intensity. Reproduced with permission from Refs. [28,38,39]. Royal Society of Chemistry, 2019, Springer, 2020, and American Society of Chemistry, 2020.

- i.  $\text{CH}_3\text{OH}(\text{g}) + \text{HO}(\text{s}) \leftrightarrow \text{CH}_3\text{O}(\text{a}) + \text{H}_2\text{O}(\text{s})$
- ii.  $\text{CH}_3\text{O}(\text{a}) + \text{O}_\text{L} \rightarrow \text{HCHO}(\text{a}) + \text{HO}(\text{s}) + \text{V}_\text{O}$
- iii.  $\text{CH}_3\text{O}(\text{g}) + \text{HCHO}(\text{a}) \rightarrow \text{CH}_3\text{OCH}_2\text{O}(\text{a})$
- iv.  $\text{CH}_3\text{OCH}_2\text{O}(\text{a}) + \text{HO}(\text{s}) \rightarrow \text{CH}_3\text{OCOH}(\text{a}) + \text{H}_2\text{O}(\text{a})$
- v.  $\text{V}_\text{O} + 0.5 \text{O}_2(\text{s}) \rightarrow \text{O}_\text{L}$

Notes: (g), gas phase; (s), surface species; (a), adsorbed species;  $\text{O}_\text{L}$ , oxygen lattice;  $\text{V}_\text{O}$ , oxygen vacancies.

**Scheme 1.** Main steps in methanol photo-oxidation to methyl formate over photocatalysts.

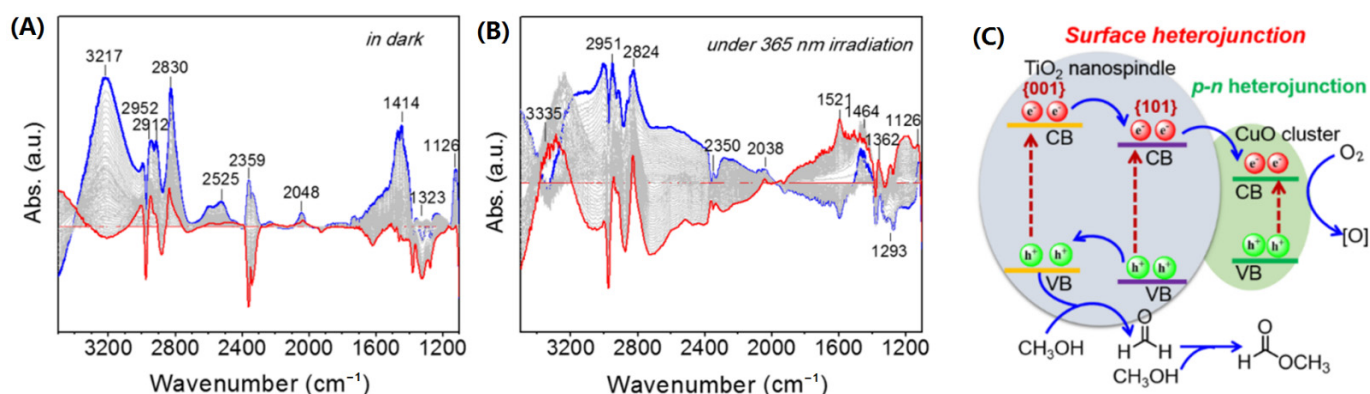


**Figure 5.** ATR-IR spectra of  $\text{CuO}/\text{TiO}_2$  in the dark (A) and under a 365 nm light (B). (C) Tentative mechanism. Reproduced with permissions from Ref. [38]. Springer, 2019.

Further, Figure 5C figured out the proposed mechanism over  $\text{CuO}/\text{TiO}_2$  composites. The electrons are formed at  $\text{TiO}_2$ 's valence band by the UV irradiation, which transfers to its conduction band, resulting in electrons and holes. The accumulated electrons would

be transferred to the CuO surface via a p-n heterojunction, which largely improves the separation efficiency of photo-generated electrons and holes. The generated holes promote the HCHO\* formation by CH<sub>3</sub>OH oxidation. In contrast, the dissociation of oxygen occurred over CuO particles with the aid of the generated electrons to refill TiO<sub>2</sub> oxygen vacancies (Scheme 1), which is the rate-determining step during the methanol photo-oxidation [39,41].

Table 1 summarizes and compares the catalytic performances, including CH<sub>3</sub>OH conversion, selectivity toward methyl formate, and formation rate of methyl formate, over these reported photocatalysts in the selective photo-oxidation of methanol into methyl formate (in the gas phase at room temperature). Surprisingly, the CH<sub>3</sub>OH conversion was largely promoted when the IB metal NPs, particularly the Cu species, were immobilized on the surface of TiO<sub>2</sub>.

**Table 1.** Comparison of the methyl formate synthesis via photo-oxidation at ambient temperature (25 °C).

Photocatalysts	CH <sub>3</sub> OH Conversion	Methyl Formate Selectivity	Methyl Formate Formation Rate (mmol <sub>CH<sub>3</sub>OH</sub> g <sub>cat.</sub> <sup>-1</sup> h <sup>-1</sup> )	Refs.
A-TiO <sub>2</sub>	10%	91%	1.5	[30]
P25	27%	56%	1.8	[42]
Ag/TiO <sub>2</sub>	75%	80%	7.3	[42]
Au/TiO <sub>2</sub>	65%	75%	5.9	[42]
Cu/TiO <sub>2</sub>	65%	55%	4.4	[32]
CuO/CuZnAl	80%	60%	5.8	[43]
Pd-Cu/TiO <sub>2</sub> -P90	53%	80%	5.7	[44]
CuO/TiO <sub>2</sub> -S	95%	84%	10.8	[29]
CuO/TiO <sub>2</sub> -P	97%	83%	10.5	[38]
CuO/TiO <sub>2</sub> -T	93%	90%	22.9	[39]

### 3. Ethanol Conversion

#### 3.1. Hydrocarbons (Biofuels) via Thermal Reactions

In the transportation sector, liquid fuel is one of the important sources of energy. It can be traditionally achieved from fossil-based resources on an industrial scale. In recent decades, with the rapid emergence of renewable biomass energy, the plant-based industry is a new opportunity for producing sustainable biofuels with a high-energy density. It exhibits a similar chemical structure to liquid fuel [45–48]. The production of biofuels has attracted particular interest. Bioethanol, known as “cellulosic ethanol”, appears as a green and important chemical, which can be obtained from various plant materials [10], and the ethanol can react with aldehydes via the cross-aldol condensation in the presence of various base catalysts [49]. The cross-aldol condensation usually is viewed as an effective method to synthesize biofuels via C–C bond formations. Currently, this method extends to oxidation condensation, which could provide a new platform for hydrocarbon biofuels production [50,51].

The preparation of C9-C13 biofuels with cellulosic ethanol in the liquid phase has emerged as a promising and versatile protocol, Figure 6. The supported nanogold catalysts exhibited excellent catalytic activity in ethanol oxidation with cinnamaldehyde. It finally gave the C11-C13 hydrocarbons [52]. A selectivity as high as 70% for C11-C13 hydrocarbon could be achieved by the Au/NiO catalyst via a one-pot cascade reaction, viz. cross aldol condensations using K<sub>2</sub>CO<sub>3</sub> as cocatalyst, Figure 7 [53]. Then it was via a full hydrodeoxygenation with hydrogen gas. The ethanol was activated to acetaldehyde (CH<sub>3</sub>CHO\*) at the sites of NiO oxide’s oxygen vacancies, supported by EtOH-TPD and TGA analyses. Then the CH<sub>3</sub>CHO\* reacts with cinnamaldehyde at the interfacial perimeter of the Au/NiO composite during the cascade reactions. The whole catalytic conversions were monitored by in situ infrared spectroscopy investigations.

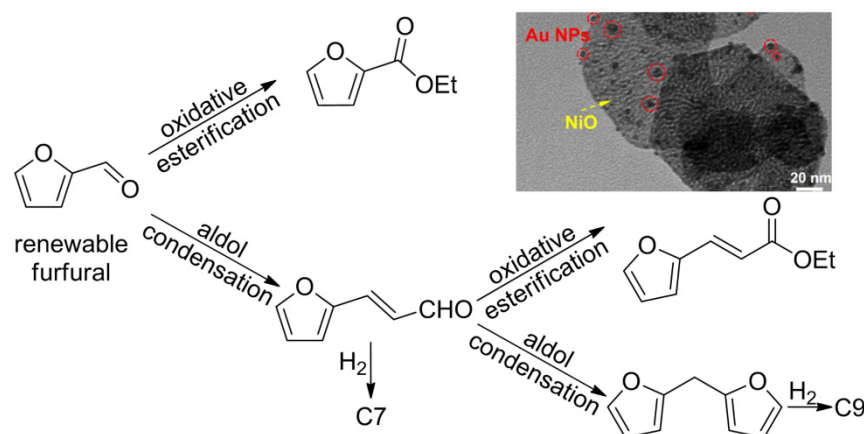


**Figure 6.** Conversion pathway of biomass furfural to C7-9 hydrocarbons over the Au/NiO catalysts (Inset, TEM image). Reproduced with permission from Ref. [52]. American Chemical Society, 2019.

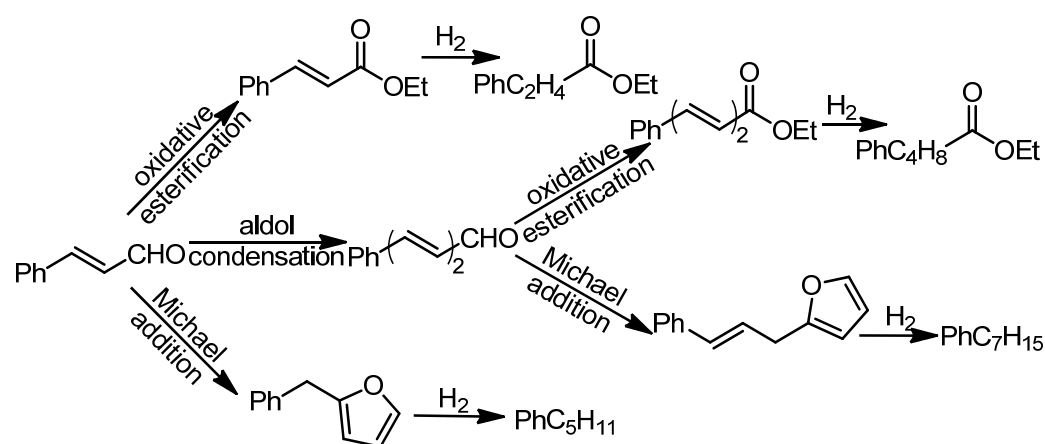


**Figure 7.** Conversion pathway from cinnamaldehyde to C11-13 hydrocarbons. Reproduced with permission from Ref. [49]. Royal Society of Chemistry, 2019.

### 3.2. Ethanal via Photocatalysis

The atomically precise metal nanoclusters with certain crystal structures have been synthesized as a kind of well-defined model nanocatalysts in selective oxidations [54–56]. The mono-dopant into a metal particle at a specific position can well tailor its electronic property and thus modify its catalytic performances. For example, Qin and coworkers developed a strategy to dope a mono-Ag-atom at the central site of rod-shaped  $\text{Au}_{13}\text{Ag}_{12}(\text{PPh}_3)_{10}\text{Cl}_8$  nanoclusters to a “pigeon-pair” cluster of  $\{[\text{Au}_{13}\text{Ag}_{12}(\text{PPh}_3)_{10}\text{Cl}_8] \cdot [\text{Au}_{12}\text{Ag}_{13}(\text{PPh}_3)_{10}\text{Cl}_8]\}^{2+}$  [57,58]. The single-atom exchange between  $\text{Au}_{13}\text{Ag}_{12}$  and  $\text{Au}_{12}\text{Ag}_{13}$  nanoclusters induced a significant perturbation to the electronic structure, which can result in a difference in catalytic activity [59–61]. Thus,  $\text{Au}_{13}\text{Ag}_{12}$  and  $\text{Au}_{13}\text{Ag}_{12} \cdot \text{Au}_{12}\text{Ag}_{13}$  clusters, both being supported on  $\text{TiO}_2$ , were used in the photocatalytic conversion of ethanol in order to compare the catalytic performance [62]. The cluster catalysts were evaluated in the selective aerobic oxidation of ethanol gas under a UV irradiation at 30 °C.  $\text{Au}_{13}\text{Ag}_{12} \cdot \text{Au}_{12}\text{Ag}_{13}$  clusters gave a higher ethanol conversion (34%), which is ~1.5-fold over that of the  $\text{Au}_{13}\text{Ag}_{12}$  clusters (23%), Figure 8B. Further, the selectivity toward ethanal on the  $\text{Au}_{13}\text{Ag}_{12} \cdot \text{Au}_{12}\text{Ag}_{13}$  clusters (79%) is slightly higher than that on  $\text{Au}_{13}\text{Ag}_{12}$  clusters (72%), but the product distribution is very similar for two catalysts, suggesting that the conversion mechanism over both catalysts should be same. In all, the single-atom exchange (Au for Ag) in  $\text{M}_{25}$  clusters lead to distinct electronic properties indeed makes a significant influence on the catalytic activity.

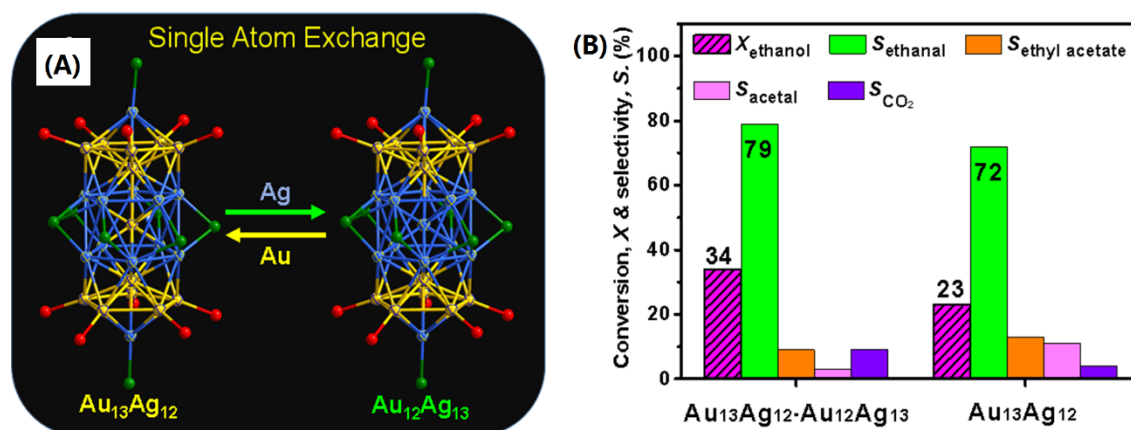


**Figure 8.** (A) Metal-exchanging at the central site of M25 clusters. (B) Photocatalytic performance in the ethanol conversion. Reproduced with permission from Ref. [53]. Springer, 2022.

#### 4. Oxidation of D-Glucose to Gluconic Acid

The activated carbon (AC) supported Au nanoparticles have previously been reported as a catalyst for selective aerobic oxidation of D-glucose to gluconic acid [63–66]. This result prompted the investigation of the catalytic performance of AC-supported  $Au_{38}(SR)_{24}$  for the oxidation of D-glucose [67]. Impressively, the annealed sample of  $Au_{38}(SR)_{24}/AC-120$  catalyst showed high activity and better catalytic performance than  $Au_{38}/AC-150$  and  $Au_{38}/AC-300$  (120, 150, and 300 °C indicates the annealing temperature in the air). It has been demonstrated that the desorption of thiol occurs at ~200 °C, which suggests that the partial removal of thiols in  $Au_{38}(SR)_{24}/AC-120$  catalyst provides highly active sites than more thiol ligands removal at 150 °C or the complete removal of thiols at 300 °C. The turnover frequency (TOF) for  $Au_{38}(SR)_{24}/AC-120$  was  $\sim 5440 \text{ h}^{-1}$ , which is found to be even higher than the commercially available Pd/AC, Pd-Bi/AC, and Au/AC. Furthermore, excellent recyclability also could be found with  $Au_{38}(SR)_{24}/AC-120$  catalyst.

The reasonable reaction mechanism for the above-described aerobic oxidation of D-glucose catalyzed by  $Au_{25}(SR)_{18}/AC$  is shown in Figure 6. Here, the terminal -CHO group of D-glucose molecule first selectively adsorbs on the staple of  $Au_n(SR)_m$  clusters, and  $O_2$  is activated on activated carbon in the presence of bases simultaneously. Subsequently, -CHO is selectively oxidized to the -COOH/-COO<sup>-</sup> group. In the last, gluconates desorbed and detached from the Au clusters in the alkaline medium. Thus, the staple motif has a critical role to play here in enhancing the catalytic activity. Further,  $Au_{25}(SR)_{18}$  (1.1 nm),  $Au_{38}(SR)_{24}$  (1.2 nm), and  $Au_{144}(SR)_{60}$  (1.7 nm) were used to exemplify the size dependence of Au nanocluster catalysts [68]. Experimental results showed that all clusters have excellent catalytic activity with 98% selectivity and follow the order:  $Au_{144}(SR)_{60}/AC > Au_{38}(SR)_{24}/AC > Au_{25}(SR)_{18}/AC$  (equal moles of nanoclusters, the molar ratio of glucose/NC was fixed at 18,000:1). Rationally, the above size dependence is attributed to the effect of the core size of metal nanoclusters.

At the same time, Guo et al. [69] prepared  $TiO_2$ -supported ultrasmall gold cluster catalysts (particle's size: 1.2–1.7 nm) with a simple incipient wetness method and used anthranilic acid as a stabilizing agent. Surprisingly, The  $Au/TiO_2$  with surface  $Au^{\delta+}$  species (annealed at 200 and 500 °C in the air), corroborated by XPS and Operando-DRIFTS analyses (Figure 9B), showed inactive in the base-free reaction condition for oxidation of glucose. However, the  $Au/TiO_2$  with only surface metallic  $Au^0$  species (annealed at 150 and 200 °C in the presence of  $H_2$  gas) exhibited salient catalytic performance (87–92% conversion and 95–97% selectivity for gluconic acid), revealing that the metallic  $Au^0$  sites are very important for glucose oxidation in this reaction system. Note that the by-product in the oxidation was fructose by isomerization of glucose (Figure 9A). The turnover frequency of  $Au/TiO_2$  could be achieved to  $1908 \text{ mol}_{\text{reacted glucose}} \text{ mol}_{Au}^{-1} \text{ h}^{-1}$ , which is 1.5-fold of the commercial Pd-Bi/C catalysts with alkaline existence (TOF:  $1298 \text{ mol}_{\text{reacted glucose}} \text{ mol}_{Pd}^{-1} \text{ h}^{-1}$ ,

NaOH solution with a pH 9.5), and the apparent activation energies are comparable to the unsupported Au clusters, also indicating that the oxidation should occur at Au surface rather than at the perimeter interface between Au clusters and supports (Figure 9C). This study gave some clues that the metallic gold particle is the catalytically active center for the aerobic glucose oxidation conversion to gluconic acid.

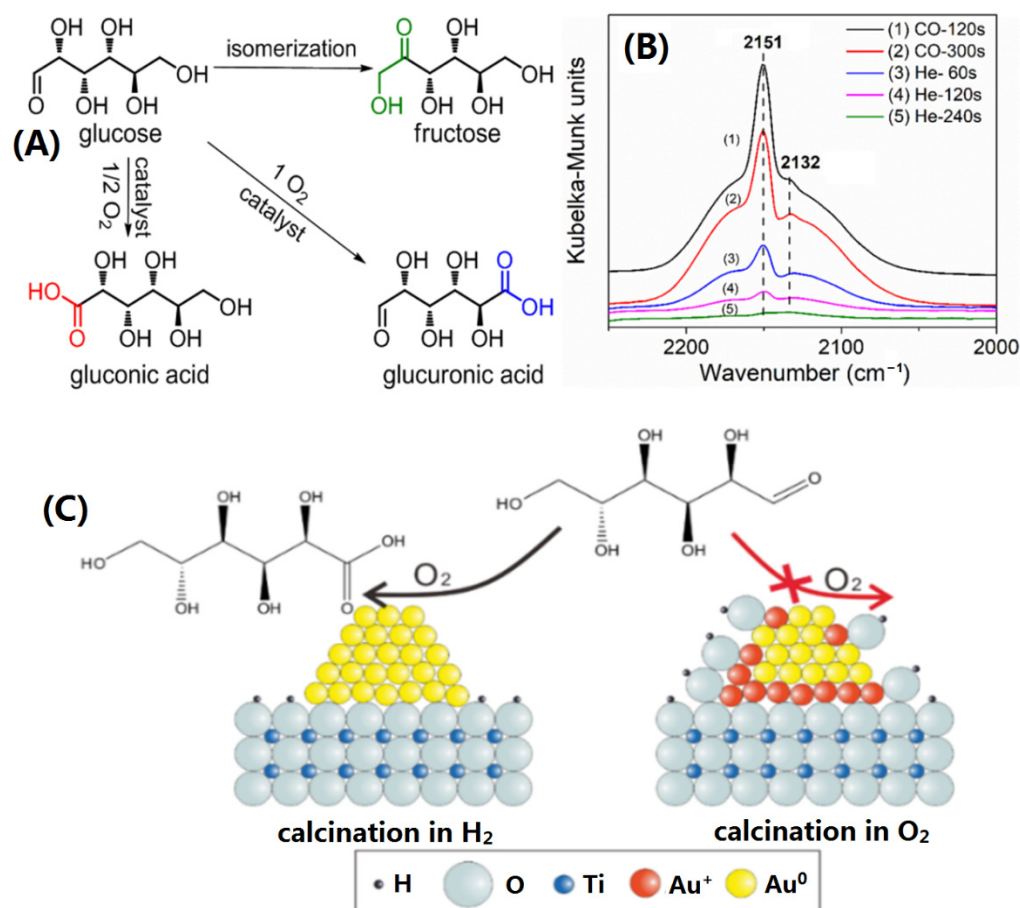


**Figure 9.** (A) Isomerization of glucose and fructose and the glucose conversion to gluconic acid via aerobic oxidations. (B) Operando-DRIFTS CO adsorption over Au/TA-200 catalysts at  $-150$  °C. (C) Plausible mechanism for the aerobic oxidation. Reproduced with permission from Ref. [69]. Royal Society of Chemistry, 2019.

## 5. Conclusions, Challenges, and Future Perspective

We fabricated the aerobic oxidation of biomass into highly valuable chemicals via green catalytic systems over the supported copper and gold nanoclusters catalysts, which led to some significant breakthroughs, as highlighted below:

- (1) Three types of oxidations were achieved, photo-oxidation of methanol to methyl formate over CuO<sub>x</sub>/TiO<sub>2</sub> nanocomposites, ethanol to hydrocarbons biofuels over Au/NiO, and glucose oxidation to gluconic acid catalyzed by Au/activated carbon.
- (2) The titania supports copper oxide clusters with different morphology of nanosheets, nanospindles, and nanotubes have been designed to investigate the catalytic performance in the photo-oxidation reaction of the method.
- (3) The active-site identification and creation in the aerobic oxidation were exemplified. The CuO<sub>x</sub>/TiO<sub>2</sub>[101] interface was identified in the photo-oxidation of methanol, and only the metallic Au<sup>0</sup> clusters were clarified to be active-site for the glucose oxidation.
- (4) It has been observed that the single-atom-exchanging in the metal clusters largely affects the catalytic activity instead of product selectivity. However, the detailed mechanism is still unknown.

- (5) By the ATR-IR spectra method, we clearly mapped out the whole conversion pathway and worked out the controversy in this photocatalysis.

However, there are still some following points for utmost consideration:

- (1) In the future, more efforts must be put into creating novel photo/catalysts with specific active reaction sites for biomass conversions [70,71].
- (2) In the future, sincere efforts will be put forward to develop more biomass conversion systems.
- (3) DFT studies with in situ characterizations must be advanced to establish plausible reaction mechanisms.
- (4) Attempts must be made to increase the reaction scales to meet the industrial needs, especially the photo-oxidation reactions [72].
- (5) Alloy metal nanoparticle catalysts need to be exploited in the biomass conversions, as the electronic property can be well modified to tailor their catalytic performances.
- (6) Finally, in the near future, we will try to expand our horizons in other different fields of catalysis [73–75].

**Author Contributions:** Investigation, Y.Z. and C.C.; resources, Y.Z. and C.C.; writing—original draft preparation, Y.Z., C.C. and G.L.; writing—review and editing, G.L.; supervision, G.L.; project administration, C.C. and G.L. All authors have read and agreed to the published version of the manuscript.

**Funding:** This research received no external funding.

**Institutional Review Board Statement:** The study was conducted in accordance with the Declaration of Helsinki, and approved by the Institutional Review Board.

**Informed Consent Statement:** Not applicable.

**Conflicts of Interest:** The authors declare no conflict of interest.

## References

1. Lee, J.S.; Kim, J.; Kim, Y. Methyl formate as a new building block in C1 chemistry. *Appl. Catal.* **1990**, *57*, 1–30. [[CrossRef](#)]
2. Nwosu, U.; Wang, A.; Palma, B.; Zhao, H.; Khan, M.A.; Kibria, M.; Hu, J. Selective biomass photoreforming for valuable chemicals and fuels: A critical review. *Renew. Sustain. Energy Rev.* **2021**, *148*, 111266. [[CrossRef](#)]
3. Guo, Y.L.; Lu, G.Z.; Mo, X.H.; Wang, Y.S. Vapor phase dehydrogenation of methanol to methyl formate in the catalytic membrane reactor with Cu/SiO<sub>2</sub>/ceramic composite membrane. *Catal. Lett.* **2005**, *99*, 105–108. [[CrossRef](#)]
4. Chen, Y.; Li, Y.; Chen, W.; Xu, W.W.; Han, Z.-K.; Waheed, A.; Ye, Z.; Li, G.; Baiker, A. Continuous Di-methyl Carbonate Synthesis from CO<sub>2</sub> and Methanol over BixCe<sub>1-x</sub>O<sub>δ</sub> Monoliths: Effect of Bismuth Doping on Population of Oxygen Vacancies, Activity, and Reaction Pathway. *Nano Res.* **2022**, *15*, 1366–1374. [[CrossRef](#)]
5. Chen, Y.; Tang, Q.; Ye, Z.; Li, Y.; Yang, Y.; Pu, H.; Li, G. Monolithic Zn<sub>x</sub>Ce<sub>1-x</sub>O<sub>2</sub> catalysts for catalytic synthesis of dimethyl carbonate from CO<sub>2</sub> and methanol. *New J. Chem.* **2020**, *44*, 12522–12530. [[CrossRef](#)]
6. Tatibouët, J. Methanol oxidation as a catalytic surface probe. *Appl. Catal. A Gen.* **1997**, *148*, 213–252. [[CrossRef](#)]
7. Forzatti, P.; Tronconi, E.; Elmi, A.S.; Busca, G. Methanol oxidation over vanadia-based catalysts. *Appl. Catal. A Gen.* **1997**, *157*, 387–408. [[CrossRef](#)]
8. Chen, Y.; Wang, H.; Qin, Z.; Tian, S.; Ye, Z.; Ye, L.; Abroshan, H.; Li, G. TixCe<sub>1-x</sub>O<sub>2</sub> Nanocomposites: A Monolithic Catalyst for Direct Conversion of Carbon Dioxide and Methanol to Dimethyl Carbonate. *Green Chem.* **2019**, *21*, 4642–4649. [[CrossRef](#)]
9. Kou, H.; Lu, C.H.; Wang, J.; Chen, Y.K.; Xu, Z.Z.; Varma, R.S. Selectivity Enhancement in Heterogeneous Photocatalytic Transformations. *Chem. Rev.* **2017**, *117*, 1445–1514. [[CrossRef](#)]
10. Badwal, S.P.S.; Giddey, S.; Kulkarni, A. Direct ethanol fuel cells for transport and stationary applications—A comprehensive review. *Appl. Energy* **2015**, *145*, 80–103. [[CrossRef](#)]
11. Yin, C.; Liu, S.; Qin, Z.; Zhang, Y.; Li, G.; Zhao, Z. Butterfly-Like Tetranuclear Copper(I) Clusters for Efficient Alkyne Homocoupling Reactions. *Eur. J. Inorg. Chem.* **2020**, *2021*, 392–397. [[CrossRef](#)]
12. Shi, Q.; Qin, Z.; Ping, G.; Liu, S.; Xu, H.; Li, G. Alkynyl- and Phosphine-Ligated Quaternary Au<sub>2</sub>Ag<sub>2</sub> Clusters Featuring an Alkynyl-AuAg Motif for Multicomponent Coupling. *RSC Adv.* **2020**, *10*, 21650–21655. [[CrossRef](#)] [[PubMed](#)]
13. Subrahmanyam, A.V.; Thayumanavan, S.; Huber, G.W. C-C Bond Formation Reactions for Bio-mass-Derived Molecules. *ChemSusChem* **2010**, *3*, 1158–1161. [[CrossRef](#)] [[PubMed](#)]
14. Shi, Q.; Qin, Z.; Xu, H.; Li, G. Heterogeneous Cross-Coupling over Gold Nanoclusters. *Nanomaterials* **2019**, *9*, 838. [[CrossRef](#)]
15. Liu, Z.; Tong, X.; Liu, J.; Xue, S. A smart catalyst system for the valorization of renewable furfural in aliphatic alcohols. *Catal. Sci. Technol.* **2015**, *6*, 1214–1221. [[CrossRef](#)]

16. Ning, L.; Liao, S.; Cui, H.; Yu, L.; Tong, X. Selective Conversion of Renewable Furfural with Ethanol to Produce Furan-2-acrolein Mediated by Pt@MOF-5. *ACS Sustain. Chem. Eng.* **2017**, *6*, 135–142. [[CrossRef](#)]
17. Zhou, Y.; Li, G. A Critical Review on Carbon-Carbon Coupling over Ultra-Small Gold Nanoclusters. *Acta Phys.-Chim. Sin.* **2017**, *33*, 1297–1309. [[CrossRef](#)]
18. Cavani, F.; Albonetti, S.; Basile, F.; Gandini, A. *Chemicals and Fuels from Bio-Based Building Blocks*; Wiley-VCH: Weinheim, Germany, 2016.
19. Wang, F.; Wen, Z.; Qin, Z.; Fang, Q.; Ge, Q.; Li, Z.; Sun, J.; Li, G. Manganese cluster induce the control synthesis of RHO- and CHA-type silicoaluminophosphates for dimethylether to light olefin conversion. *Fuel* **2019**, *244*, 104–109. [[CrossRef](#)]
20. Delidovich, I.; Hausoul, P.J.C.; Deng, L.; Pfitzenreuter, R.; Rose, M.; Palkovits, R. Alternative Monomers Based on Lignocellulose and Their Use for Polymer Production. *Chem. Rev.* **2015**, *116*, 1540–1599. [[CrossRef](#)]
21. Wen, Z.; Li, Z.; Ge, Q.; Zhou, Y.; Sun, J.; Abroshan, H.; Li, G. Robust nickel cluster@Mes-HZSM-5 composite nanostructure with enhanced catalytic activity in the DTG reaction. *J. Catal.* **2018**, *363*, 26–33. [[CrossRef](#)]
22. Ping, G.; Zheng, K.; Fang, Q.; Li, G. Composite Nanostructure of Manganese Cluster and CHA-Type Sili-coaluminophosphates: Enhanced Catalytic Performance in Dimethylether to Light Olefins Conversion. *Nanomaterials* **2021**, *11*, 24. [[CrossRef](#)] [[PubMed](#)]
23. Biella, S.; Prati, L.; Rossi, M. Selective Oxidation of D-Glucose on Gold Catalyst. *J. Catal.* **2002**, *206*, 242–247. [[CrossRef](#)]
24. Anastasiadis, S.; Morgunov, I.G. Recent Pat. *Biotechnology* **2007**, *1*, 167–180.
25. Hanson, A.D.; Roje, S. One-carbon metabolism in higher plants. *Annu. Rev. Plant Physiol. Plant Mol. Biol.* **2001**, *52*, 119–137. [[CrossRef](#)]
26. Liu, J.; Zhan, E.; Cai, W.; Li, J.; Shen, W. Methanol Selective Oxidation to Methyl Formate over  $\text{ReO}_x/\text{CeO}_2$  Catalysts. *Catal. Lett.* **2007**, *120*, 274–280. [[CrossRef](#)]
27. Kaiser, D.; Beckmann, L.; Walter, J.; Bertau, M. Conversion of Green Methanol to Methyl Formate. *Catalysts* **2021**, *11*, 869. [[CrossRef](#)]
28. Shi, Q.; Wei, X.; Raza, A.; Li, G. Recent Advances in Aerobic Photo-Oxidation of Methanol to Valuable Chemicals. *ChemCatChem* **2021**, *13*, 3381–3395. [[CrossRef](#)]
29. Shi, Q.; Ping, G.; Wang, X.; Xu, H.; Li, J.; Cui, J.; Abroshan, H.; Ding, H.; Li, G. CuO/TiO<sub>2</sub> heterojunction composites: An efficient photocatalyst for selective oxidation of methanol to methyl formate. *J. Mater. Chem. A* **2019**, *7*, 2253–2260. [[CrossRef](#)]
30. Wittstock, A.; Zielasek, V.; Biener, J.; Friend, C.M.; Baumer, M. Nanoporous Gold Catalysts for Selective Gas-Phase Oxidative Coupling of Methanol at Low Temperature. *Science* **2010**, *327*, 319–322. [[CrossRef](#)]
31. Kominami, H.; Sugahara, H.; Hashimoto, K. Photocatalytic selective oxidation of methanol to methyl formate in gas phase over titanium(IV) oxide in a flow-type reactor. *Catal. Commun.* **2010**, *11*, 426–429. [[CrossRef](#)]
32. Liu, J.; Han, C.; Yang, X.; Gao, G.; Shi, Q.; Tong, M.; Liang, X.; Li, C. Methyl formate synthesis from methanol on titania supported copper catalyst under UV irradiation at ambient condition: Performance and mechanism. *J. Catal.* **2016**, *333*, 162–170. [[CrossRef](#)]
33. Russier, V.; Badiali, J. Calculation of the electronic work function of Cu and Ag from an extended jellium model. *Phys. Rev. B* **1989**, *39*, 13193. [[CrossRef](#)] [[PubMed](#)]
34. Guo, S.; Zhang, S.H.; Fang, Q.H.; Abroshan, H.D.; Kim, H.; Haruta, M.; Li, G. Gold-Palladium Nanoparticles Supported by Graphene Oxide and Lamellar TiO<sub>2</sub> for Direct Synthesis of Hydrogen Peroxide. *ACS Appl. Mater. Interfaces* **2018**, *10*, 40599–40607. [[CrossRef](#)] [[PubMed](#)]
35. Kollhoff, F.; Schneider, J.; Li, G.; Barkaoui, S.; Shen, W.; Berger, T.; Diwald, O.; Libuda, J. Anchoring of carboxyl-functionalized porphyrins on MgO, TiO<sub>2</sub>, and Co<sub>3</sub>O<sub>4</sub> nanoparticles. *Phys. Chem. Chem. Phys.* **2018**, *20*, 24858–24868. [[CrossRef](#)]
36. Shao, B.; Zhao, W.; Miao, S.; Huang, J.; Wang, L.; Li, G.; Shen, W. Facet-dependent anchoring of gold nanoparticles on TiO<sub>2</sub> for CO oxidation. *Chin. J. Catal.* **2019**, *40*, 1534–1539. [[CrossRef](#)]
37. Chen, H.; Liu, C.; Wang, M.; Zhang, C.; Luo, N.; Wang, Y.; Abroshan, H.; Li, G.; Wang, F. Visible Light Gold Nanocluster Photocatalyst: Selective Aerobic Oxidation of Amines to Imines. *ACS Catal.* **2017**, *7*, 3632–3638. [[CrossRef](#)]
38. Shi, Q.Q.; Qin, Z.X.; Yu, C.L.; Waheed, A.; Xu, H.; Gao, Y.; Abroshan, H.; Li, G. Experimental and mechanistic understanding of photo-oxidation of methanol catalyzed by CuO/TiO<sub>2</sub>-spindle nano-composite: Oxygen vacancy engineering. *Nano Res.* **2020**, *13*, 939–946. [[CrossRef](#)]
39. Zhang, S.; Gong, X.; Shi, Q.; Ping, G.; Xu, H.; Waleed, A.; Li, G. CuO Nanoparticle-Decorated TiO<sub>2</sub>-Nanotube Heterojunctions for Direct Synthesis of Methyl Formate via Photo-Oxidation of Methanol. *ACS Omega* **2020**, *5*, 15942–15948. [[CrossRef](#)]
40. Shi, Q.; Wang, Y.; Guo, S.; Han, Z.-K.; Ta, N.; Li, G.; Baiker, A. NO reduction with CO over CuOx/CeO<sub>2</sub> Nanocomposites: Influence of Oxygen Vacancies and Lattice Strain. *Catal. Sci. Technol.* **2021**, *11*, 6543–6552. [[CrossRef](#)]
41. Li, W.L.; Liu, C.; Abroshan, H.D.; Ge, Q.J.; Yang, X.J.; Xu, H.Y.; Li, G. Catalytic CO Oxidation Using Bimetallic M<sub>x</sub>Au<sub>25-x</sub> Clusters: A Combined Experimental and Computational Study on Doping Effects. *J. Phys. Chem. C* **2016**, *120*, 10261–10267. [[CrossRef](#)]
42. Han, C.; Yang, X.; Gao, G.; Wang, J.; Lu, H.; Liu, J.; Tong, M.; Liang, X. Selective oxidation of methanol to methyl formate on catalysts of Au–Ag alloy nanoparticles supported on titania under UV irradiation. *Green Chem.* **2014**, *16*, 3603–3615. [[CrossRef](#)]
43. Liang, X.Y.; Yang, X.Z.; Gao, G.J.; Li, C.F.; Li, Y.Y.; Zhang, W.D.; Chen, X.T.; Zhang, Y.B.; Zhang, B.B.; Lei, Y.Q.; et al. Performance and mechanism of CuO/CuZnAl hydrotalcites-ZnO for photo-catalytic selective oxidation of gaseous methanol to methyl formate at ambient temperature. *J. Catal.* **2016**, *339*, 68–76. [[CrossRef](#)]

44. Lisowski, P.; Colmenares, J.C.; Łomot, D.; Chernyayeva, O.; Lisovytskiy, D. Preparation by sonophotodeposition method of bimetallic photocatalysts Pd-Cu/TiO<sub>2</sub> for sustainable gaseous selective oxidation of methanol to methyl formate. *J. Mol. Catal. A Chem.* **2016**, *411*, 247–256. [[CrossRef](#)]
45. Alonso, D.M.; Bond, J.Q.; Dumesic, J.A. Catalytic conversion of biomass to biofuels. *Green Chem.* **2010**, *12*, 1493–1513. [[CrossRef](#)]
46. Oumer, A.; Hasan, M.; Baheta, A.T.; Mamat, R.; Abdullah, A. Bio-based liquid fuels as a source of renewable energy: A review. *Renew. Sustain. Energy Rev.* **2018**, *88*, 82–98. [[CrossRef](#)]
47. Zhao, C.; Brück, T.; Lercher, J.A. Catalytic deoxygenation of microalgae oil to green hydrocarbons. *Green Chem.* **2013**, *15*, 1720–1739. [[CrossRef](#)]
48. Bridgwater, A. Renewable fuels and chemicals by thermal processing of biomass. *Chem. Eng. J.* **2003**, *91*, 87–102. [[CrossRef](#)]
49. Huber, G.W.; Chheda, J.N.; Barrett, C.J.; Dumesic, J.A. Production of Liquid Alkanes by Aqueous-Phase Processing of Biomass-Derived Carbohydrates. *Science* **2005**, *308*, 1446–1450. [[CrossRef](#)]
50. Zhang, G.; Wang, R.; Li, G. Non-metallic gold nanoclusters for oxygen activation and aerobic oxidation. *Chin. Chem. Lett.* **2018**, *29*, 687–693. [[CrossRef](#)]
51. Li, G.; Jiao, W.; Sun, Z.; Zhao, Y.; Shi, Z.; Yan, Y.; Feng, L.; Zhang, Y.; Tang, Y. A Scalable Upgrading of Concentrated Furfural in Ethanol: Combining Meerwein–Ponndorf–Verley Reduction with in Situ Cross Aldol Condensation. *ACS Sustain. Chem. Eng.* **2018**, *6*, 4316–4320. [[CrossRef](#)]
52. Fang, Q.; Qin, Z.; Shi, Y.; Liu, F.; Barkaoui, S.; Abroshan, H.; Li, G. Au/NiO Composite: A Catalyst for One-Pot Cascade Conversion of Furfural. *ACS Appl. Energy Mater.* **2019**, *2*, 2654–2661. [[CrossRef](#)]
53. Shi, Y.; Tian, S.; Shi, Q.; Waheed, A.; Cao, Y.; Li, G. Cascade aldol condensation of an aldehyde via the aerobic oxidation of ethanol over an Au/NiO composite. *Nanoscale Adv.* **2019**, *1*, 3654–3659. [[CrossRef](#)]
54. Shi, Q.; Qin, Z.; Sharma, S.; Li, G. Recent Progress in Heterogeneous Catalysis by Atomically and Structurally Precise Metal Nanoclusters. *Chem. Rec.* **2021**, *21*, 879–892. [[CrossRef](#)] [[PubMed](#)]
55. Zheng, K.; Zhang, J.; Zhao, D.; Yang, Y.; Li, Z.; Li, G. Motif-mediated Au<sub>25</sub>(SPh)<sub>5</sub>(PPh<sub>3</sub>)<sub>10</sub>X<sub>2</sub> nanorods with conjugated electron delocalization. *Nano Res.* **2018**, *12*, 501–507. [[CrossRef](#)]
56. Qin, Z.; Sharma, S.; Wan, C.-Q.; Malola, S.; Xu, W.-W.; Häkkinen, H.; Li, G. A Homoleptic Alkynyl-Ligated [Au<sub>13</sub>Ag<sub>16</sub>L<sub>24</sub>]<sub>3</sub>-Cluster as a Catalytically Active Eight-Electron Superatom. *Angew. Chem. Int. Ed.* **2020**, *59*, 970–975.
57. Qin, Z.; Zhang, J.; Wan, C.; Liu, S.; Abroshan, H.; Jin, R.; Li, G. Atomically precise nanoclusters with reversible isomeric transformation for rotary nanomotors. *Nat. Commun.* **2020**, *11*, 1–6. [[CrossRef](#)]
58. Qin, Z.; Hu, S.; Han, W.; Li, Z.; Xu, W.W.; Zhang, J.; Li, G. Tailoring optical and photocatalytic properties by single-Ag-atom exchange in Au<sub>13</sub>Ag<sub>12</sub>(PPh<sub>3</sub>)<sub>10</sub>Cl<sub>8</sub> nanoclusters. *Nano Res.* **2021**, *15*, 2971–2976. [[CrossRef](#)]
59. Zhu, H.; Yuan, X.; Yao, Q.; Xie, J. Shining Photocatalysis by Gold-based Nanomaterials. *Nano Energy* **2021**, *88*, 106306. [[CrossRef](#)]
60. Liu, Z.; Qin, Z.; Cui, C.; Luo, Z.; Yang, B.; Jiang, Y.; Lai, C.; Wang, Z.; Wang, X.; Fang, X.; et al. In-Situ Generation and Global Property Profiling of Metal nanoclusters by Ultraviolet Laser Dissociation-Mass Spectrometry. *Sci. China Chem.* **2022**, *65*. [[CrossRef](#)]
61. Qin, Z.; Zhao, D.; Zhao, L.; Xiao, Q.; Wu, T.; Zhang, J.; Wan, C.; Li, G. Tailoring the Stability, Photocatalysis and Photoluminescence Properties of Au<sub>11</sub> Nanocluster via Doping Engineering. *Nanoscale Adv.* **2019**, *1*, 2529–2536. [[CrossRef](#)]
62. Du, X.; Huang, Y.; Pan, X.; Han, B.; Su, Y.; Jiang, Q.; Li, M.; Tang, H.; Li, G.; Qiao, B. Size-dependent strong metal-support interaction in TiO<sub>2</sub> supported Au nanocatalysts. *Nat. Commun.* **2020**, *11*, 1–8. [[CrossRef](#)] [[PubMed](#)]
63. Ishida, T.; Kinoshita, N.; Okatsu, H.; Akita, T.; Takei, T.; Haruta, M. Influence of the support and the size of gold clusters on catalytic activity for glucose oxidation. *Angew. Chem. Int. Ed.* **2008**, *47*, 9265–9268. [[CrossRef](#)] [[PubMed](#)]
64. Perovic, M.; Tarakina, N.V.; Hofmann, J.P.; Oschatz, M. Influence of Local Environments in Pores of Different Size on the Catalytic Liquid-Phase Oxidation of d-Glucose by Au Nanoparticles Supported on Nanoporous Carbon. *ACS Appl. Nano Mater.* **2020**, *3*, 7695–7703. [[CrossRef](#)]
65. Zhang, H.; Toshima, N. Glucose oxidation using Au-containing bimetallic and trimetallic nanoparticles. *Catal. Sci. Technol.* **2013**, *3*, 268–278. [[CrossRef](#)]
66. Cattaneo, S.; Stucchi, M.; Villa, A.; Prati, L. Gold Catalysts for the Selective Oxidation of Biomass-Derived Products. *ChemCatChem* **2018**, *11*, 309–323. [[CrossRef](#)]
67. Liu, C.; Zhang, J.; Huang, J.; Zhang, C.; Hong, F.; Zhou, Y.; Li, G.; Haruta, M. Efficient Aerobic Oxidation of Glucose to Gluconic Acid over Activated Carbon-Supported Gold Clusters. *ChemSusChem* **2017**, *10*, 1976–1980. [[CrossRef](#)]
68. Zhang, J.; Li, Z.; Huang, J.; Liu, C.; Hong, F.; Zheng, K.; Li, G. Size dependence of gold clusters with precise numbers of atoms in aerobic oxidation of d-glucose. *Nanoscale* **2017**, *9*, 16879–16886. [[CrossRef](#)]
69. Guo, S.; Fang, Q.; Li, Z.; Zhang, J.; Zhang, J.; Li, G. Efficient base-free direct oxidation of glucose to gluconic acid over TiO<sub>2</sub>-supported gold clusters. *Nanoscale* **2018**, *11*, 1326–1334. [[CrossRef](#)]
70. Almada, C.C.; Kazachenko, A.; Fongarland, P.; Perez, D.D.S.; Kuznetsov, B.; Djakovitch, L. Supported-Metal Catalysts in Upgrading Lignin to Aromatics by Oxidative Depolymerization. *Catalysts* **2021**, *11*, 467. [[CrossRef](#)]
71. Raza, A.; Zhang, X.; Ali, S.; Cao, C.; Rafi, A.A.; Li, G. Photoelectrochemical Energy Conversion over 2D Materials. *Photochem* **2022**, *2*, 272–298. [[CrossRef](#)]
72. Roman, K.; Barwicki, J.; Hryniewicz, M.; Szadkowska, D.; Szadkowski, J. Production of Electricity and Heat from Biomass Wastes Using a Converted Aircraft Turbine AI-20. *Processes* **2021**, *9*, 364. [[CrossRef](#)]

73. Cao, Y.; Su, Y.; Xu, L.; Yang, X.; Han, Z.; Cao, R.; Li, G. Ionic liquids modified oxygen vacancy-rich amorphous FeNi hydroxide nanoclusters on carbon-based materials as an efficient electrocatalyst for electrochemical water oxidation. *J. Energy Chem.* **2022**, *71*, 167–173. [[CrossRef](#)]
74. Shi, Q.; Zhang, X.; Liu, X.; Xu, L.; Liu, B.; Zhang, J.; Xu, H.; Han, Z.; Li, G. In-situ exfoliation and assembly of 2D/2D g-C<sub>3</sub>N<sub>4</sub>/TiO<sub>2</sub>(B) hierarchical microflower: Enhanced photo-oxidation of benzyl alcohol under visible light. *Carbon* **2022**, *196*, 401–409. [[CrossRef](#)]
75. Zhang, X.; Shi, Q.; Liu, X.; Li, J.; Xu, H.; Ding, H.; Li, G. Facile assembly of InVO<sub>4</sub>/TiO<sub>2</sub> heterojunction for enhanced photo-oxidation of benzyl alcohol. *Nanomaterials* **2022**, *12*, 1544. [[CrossRef](#)]